

Quasiclassical Trajectory Calculations for the Reaction $\text{Ne} + \text{H}_2^+ \rightarrow \text{NeH}^+ + \text{H}$

Yuliang Wang,* Baoguo Tian, Liangsheng Qu, Juna Chen, and Hui Li

Department of Basic Sciences, Naval Aeronautical and Astronautical University, Yantai 264001, PR China

*E-mail: yarmiay@163.com

Received June 29, 2011, Accepted September 28, 2011

Quasiclassical trajectory (QCT) calculations of $\text{Ne} + \text{H}_2^+$ reaction have been carried out on the adiabatic potential energy surface of the ground state $1^2 A'$. The reaction probability of the title reaction for $J = 0$ has been calculated, and the QCT result is consistent with the previous quantum mechanical wave packet result. Quasiclassical trajectory calculations of the four polarization-dependent differential cross sections have been carried out in the center of mass (CM) frame. The $P(\theta_r)$, $P(\phi_r)$ and $P(\theta_r, \phi_r)$ distributions, the $\mathbf{k}-\mathbf{k}'-\mathbf{j}'$ correlation and the angular distribution of product rotational vectors are presented in the form of polar plots. Due to the well in $1^2 A'$ PES, the reagent vibrational excitation has greater influence on the polarization of the product rotational angular momentum vectors \mathbf{j}' than the collision energy.

Key Words : Reaction stereo-dynamics, $\text{Ne} + \text{H}_2^+ \rightarrow \text{NeH}^+ + \text{H}$ reaction, Quasiclassical trajectory, Vector correlations

Introduction

The endothermic atom-molecule ion reaction has been studied extensively in the past 30 years,¹⁻¹¹ theoretically and experimentally. For the experiments, Van Pijkeren *et al.*² measured the relative energy dependent cross sections for H_2^+ ($\nu = 0-8$) using the photoelectron-secondary ion coincidence (PESICO) technique. Relative cross sections for $\nu = 0-4$ were determined as a function of translational energies in a threshold electron secondary ion coincidence (TESICO) experiment.³ Zhang *et al.*⁴ and Dressler *et al.*⁵ used the pulsed field ionization photoelectron secondary ion coincidence (PFI-PESICO) scheme to measure the integral cross sections for the two lowest reactant vibrational levels $\nu = 0$ and 1 at high signal-to-noise ratio through ion preparation using intense auto-ionization resonances. Sharp threshold onsets were observed, suggesting the importance of long-lived intermediates or resonances. And the endothermicity is 0.54 and 0.27 eV for reactant vibrational levels $\nu = 0$ and 1, respectively. They also investigated the absolute state-selected cross sections for $\nu = 0-17$ at $E_{\text{col}} = 0.7, 1.7$ and 4.5 eV. The vibrational enhancement was observed in the experiment, which was compared with quasiclassical trajectory (QCT) calculations by three distinct total energy ($E_{\text{tot}} = E_{\text{T}} + E_{\text{vib}}$) regimes. For $E_{\text{tot}} < 1$ eV, the experimental cross sections exceed the QCT results. This suggests the importance of quantum effects for lower total energy. In the aspect of theory, many groups have constructed the potential energy surface (PES)⁸⁻¹² using different methods, and many dynamics calculations have also been done. Based on the bending-corrected rotating linear model, Kress *et al.*¹³ determined the state-to-state reaction probabilities for total angular momentum $J = 0$, finding the effectivity of vibrational excitation in promoting reactivity and the extremely structured shape of the reaction probability as a function of

energy.¹⁴ Gilibert and coworkers^{15,16} calculated the state-selected integral cross sections using the coupled-states approximation (CSA), indicating the summation over J enhances the peak structure. Recently, Mayneris *et al.*¹⁸ carried out a time-dependent real wave packet (RWP) quantum study for the title reaction to determine the reaction probabilities and cross sections, presenting many resonances in $\text{Ne} + \text{H}_2^+$ proton transfer probabilities and oscillatory behavior of the cross sections. Utilizing the same method, they also studied the influence of vibrational excitation of H_2^+ and D_2^+ on the dynamics at thermal collision energies.^{2,5,19,20} In addition, the isotope effects have also been studied in both experiment and theoretical calculations. More recently, using highly correlated complete active space self-consistent field and multireference configuration interaction wave functions with a basis set of aug-cc-pV5Z, Lv *et al.*¹⁹ presented a new PES for the ground state $1^2 A'$, and performed quantum reactive scattering dynamics calculation taking the Coriolis coupling (CC) effect into account. And the results are found to be in good agreement with the experimental measurements obtained by Zhang *et al.*⁴

As mentioned above, due to its importance, it is quite necessary to study their vector properties to understand the dynamics of the $\text{Ne} + \text{H}_2^+ \rightarrow \text{NeH}^+ + \text{H}$ reaction fully, which can provide the valuable information about chemical reaction stereo-dynamics.^{17,18} In the present work, based on the global PES of the $1^2 A'$ adiabatic electronic state¹⁹ of the title reaction, we will carry out QCT calculations to investigate its vector properties. The four polarization dependent generalized differential cross-sections are also calculated. Section 2 is the brief introduction of computing scheme of QCT method; the calculation results and the related discussions are given in Section 3, and finally Section 4 concludes.

Computing Scheme

The $1^2\text{A}'$ PES used in the present work for the $\text{Ne} + \text{H}_2^+ \rightarrow \text{NeH}^+ + \text{H}$ reaction has a relatively accurate adiabatic state. It was given by Lv *et al.*,¹⁹ who fitted a set of accurate ab initio points to two- and three-body polynomial expansion in the Aguado-Paniagua functional form.²⁰ Figure 1 shows the contour plots of the three-dimensional $1^2\text{A}'$ state PES for four different Ne–H–H angles in internal coordinates for $\theta = 180^\circ, 120^\circ, 90^\circ$ and 60° . As shown in this figure, there are potential wells in the entrance valley for the different configuration. The detailed functional form and deduction process can be referred to Ref. 19.

The QCT method used here has been widely used to study dynamics of the chemical reactions.^{21–23} The classical Hamilton's equations are integrated numerically for motion in three dimensions. In the present work, the trajectory is initiated in the $v=0$ and $j=0$ levels, and the collision energies are 0.6 eV, 1.0 eV and 1.4 eV. In the calculation, a batch of 20000 trajectories is run for each energy of the $\text{Ne} + \text{H}_2^+$ and the integration step size is chosen to be 0.1 fs. For $J=0$ and $b=0$, the reaction probability is defined as $P = N_r/N$, which is the ratio of the number of reactive trajectories to the total number of trajectories. For $J \neq 0$, the impact parameter, b_{max} , is computed by calculating 20000 trajectories at a fixed value of the impact parameter b and systematically increasing the value of b until no reactive trajectories are obtained.

Later, Han *et al.* developed the stereodynamical QCT computational method,¹⁷ and the product rotational polarization of many chemical reactions^{19,21–23} has been well studied by this method. In the center-of-mass (CM) frame, the reagent relative velocity vector \mathbf{k} is parallel to the z axis while the y axis is perpendicular to the x-z plane containing the initial and final relative velocity vectors, \mathbf{k} and \mathbf{k}' . θ_i is the so-called scattering angle between the reagent relative velocity and the product relative velocity, while θ and ϕ refer to the coordinates of the unit vectors \mathbf{k}' and \mathbf{j}' along the directions of the product relative velocity and rotational

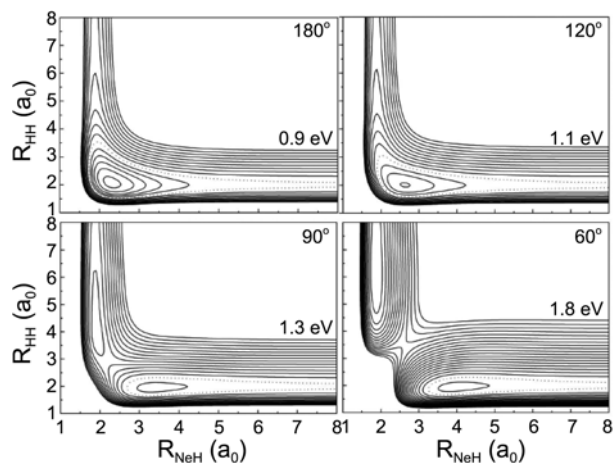


Figure 1. Contour plots of the three-dimensional $1^2\text{A}'$ state PES for four different Ne–H–H angles in internal coordinates for $\theta = 180^\circ, 120^\circ, 90^\circ$ and 60° . (taken from Ref. 19)

angular momentum vectors.

The $P(\theta_r)$ describing the $\mathbf{k}-\mathbf{j}'$ correlation which can be expanded into a series of Legendre polynomials is defined as the sum

$$P(\theta_r) = \frac{1}{2} \sum_k [k] a_0^{(k)} P_k(\cos \theta_r) \quad (1)$$

The $a_0^{(k)}$ polarization parameters are given by

$$a_0^{(k)} = \langle P_k(\cos \theta_r) \rangle \quad (2)$$

The dihedral angle distribution function $P(\phi_r)$ describing $\mathbf{k}-\mathbf{k}'-\mathbf{j}'$ correlation can be expanded as a Fourier series. In this work, $P(\theta_r)$, $P(\phi_r)$ and $P(\theta_r, \phi_r)$ are expanded up to $k=18, n=24, k=7$, which show good convergent results.

The fully correlated CM angular distribution is written as the sum

$$P(\omega_r, \omega_r) = \sum_{kq} \frac{[k]}{4\pi} \frac{1}{\sigma} \frac{d\sigma_{kq}}{d\omega_r} C_{kq}(\theta_r, \theta_r)^* \quad (3)$$

where $(1/\sigma)(d\sigma_{kq}/d\omega_r)$ is a generalized polarization dependent differential cross-section (PDDCS). In the present work, $(2\pi/\sigma)(d\sigma_{00}/d\omega_r)$, $(2\pi/\sigma)(d\sigma_{20}/d\omega_r)$, $(2\pi/\sigma)(d\sigma_{22+}/d\omega_r)$ and $(2\pi/\sigma)(d\sigma_{21-}/d\omega_r)$ are calculated.

Results and Discussion

Figure 2 shows the comparison between the time dependent wave packet (TDWP) result of the reaction probability calculated by Lv *et al.*¹⁹ and our QCT result for the reaction $\text{Ne} + \text{H}_2^+ (v=0, j=0) \rightarrow \text{NeH}^+ + \text{H} (J=0)$. As shown in this figure, the results from TDWP method and QCT method agree with each other very well in the whole collision energy range, which demonstrates the correctness of our calculation.

In order to make further investigation for the dynamics of this reaction, the vector properties have also been studied. The polarization dependent generalized differential cross-section (PDDCS) which can describe the $\mathbf{k}-\mathbf{k}'-\mathbf{j}'$ correlation and the scattering of NeH^+ has been calculated and the result

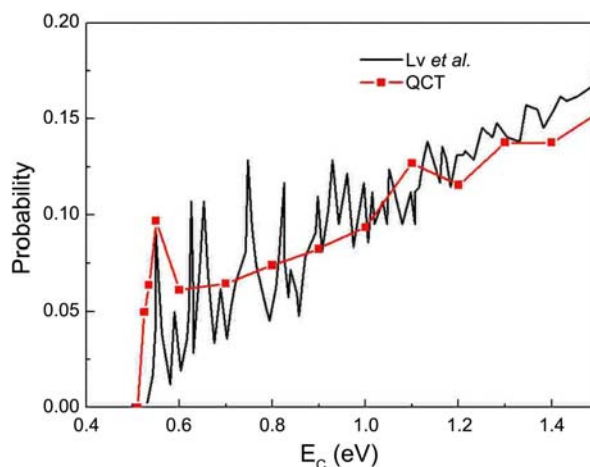


Figure 2. A comparison between the QCT-computed reaction probability in this work and the time dependent wave packet (TDWP) result calculated by Lv *et al.*¹⁹ for $\text{Ne} + \text{H}_2^+ (v=0, j=0) \rightarrow \text{NeH}^+ + \text{H} (J=0)$.

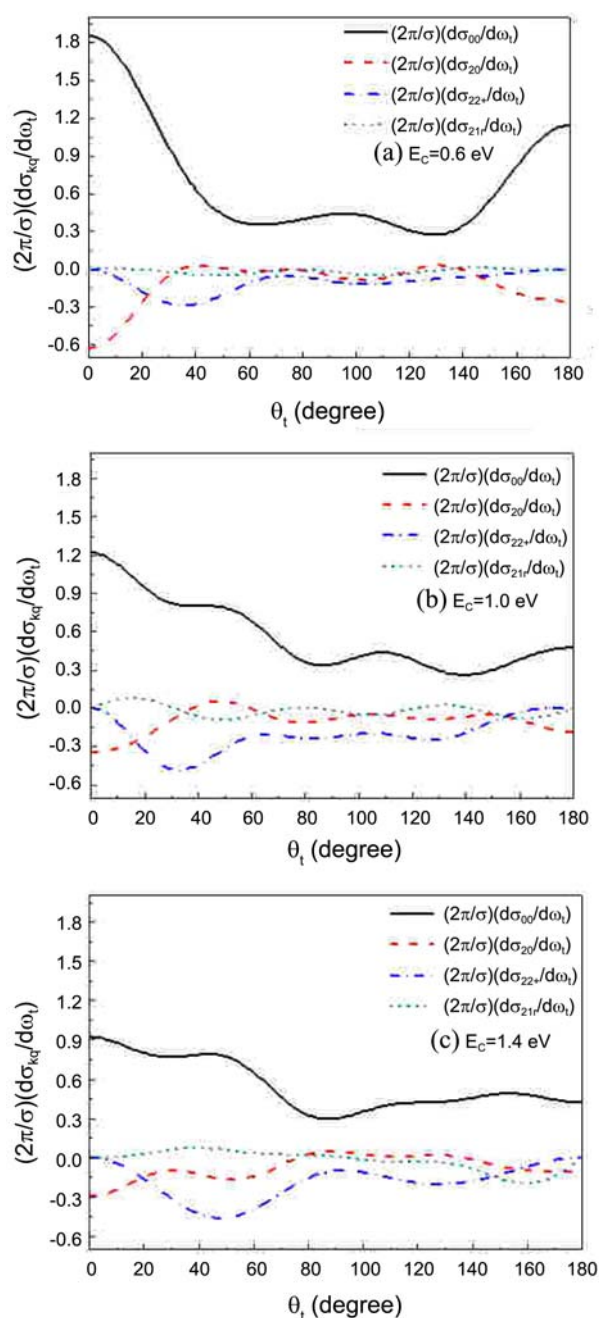


Figure 3. The polarization dependent generalized differential cross-section of the title reaction for the three different collision energies (a) $E_c = 0.6$ eV, (b) $E_c = 1.0$ eV, (c) $E_c = 1.4$ eV.

is shown in Figure 3(a), (b), and (c) with the corresponding collision energy 0.6 eV, 1.0 eV and 1.4 eV, respectively.

The PDDCS $(2\pi/\sigma)(d\sigma_{00}/d\omega_i)$ is simply the $(\mathbf{k}, \mathbf{k}')$ differential cross-section (DCS) which describes the angular distribution of the product molecule ion. It is obvious that the NeH^+ product is almost forward scattering for the three collision energies, and the tendency of forward scattering decreases with the increase in collision energy. Compared with the ones at collision energy of 1.0 eV and 1.4 eV, $(2\pi/\sigma)(d\sigma_{00}/d\omega_i)$ of the reaction at the collision energy of 0.6 eV indicates more obvious back-scattering. The PDDCS $(2\pi/\sigma)(d\sigma_{20}/d\omega_i)$ is the expectation value of the second Legendre moment $\langle P_2(\cos\theta_r) \rangle$, and the trend of it is indistinctively opposite to that of $(2\pi/\sigma)(d\sigma_{00}/d\omega_i)$. It is obvious that the PDDCSs with $q \neq 0$ are zero at the extremities of forward and backward scattering. The behavior of PDDCSs with $q \neq 0$ at the scattering away from extreme forward and backward direction is more interesting.²⁵ It provides information on the ϕ_r dihedral angle distribution. The values are nonzero at scattering angles away from $\theta_r = 0$ and π , which indicates the $P(\theta_r, \phi_r)$ distribution is not isotropic for backward scattering products. The PDDCS $(2\pi/\sigma)(d\sigma_{22+}/d\omega_i)$ is related to $\langle \sin^2\theta_r \cos 2\phi_r \rangle$, where the negative value indicates the product alignment along the y -axis, while the positive value indicates the product alignment along the x -axis. Moreover, the larger the absolute value is, the stronger is the degree of product alignment along the corresponding axis. In Figure 3, it can be seen that, with collision energy increasing, the degree of alignment along the y -axis becomes stronger at the high values of the scattering angle. When the collision energy is 0.6 eV, the value of $(2\pi/\sigma)(d\sigma_{22+}/d\omega_i)$ is clearly negative at about 35° and nearly equal to zero at the other scattering angles, indicating the slight preference of product alignment along x -axis and almost no alignment at these scattering angles, respectively. However, when the collision energy is 1.0 eV or 1.4 eV, the product is preferentially aligned along the y -axis at the wide range of scattering angles. The value of $(2\pi/\sigma)(d\sigma_{22-}/d\omega_i)$ is related to $\langle \sin^2\theta_r \cos 2\phi_r \rangle$, and it can be seen, for the three collision energies, $(2\pi/\sigma)(d\sigma_{21-}/d\omega_i)$ are nearly zero indicating the product alignment is isotropic at the wide range of scattering angles.

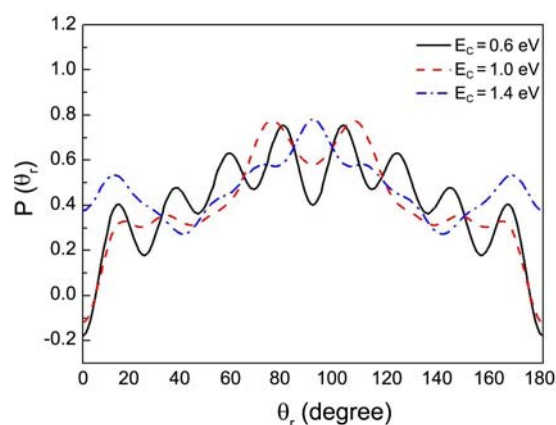


Figure 4. The distribution of $P(\theta_r)$, reflecting the $k-j'$ correlation at three collision energies.

In order to get a better graphical representation of the polarization of the NeH^+ products from the title reaction, we have plotted $P(\theta_r)$ and $P(\phi_r)$ distributions in Figure 4 and Figure 5. The $P(\theta_r)$ distribution describes the $k-j'$ correlation, which is plotted in Figure 4. It is very clearly that for 0.6 eV or 1.0 eV, $P(\theta_r)$ has no sharp peak at $\theta_r = \pi/2$, while for 1.4 eV, $P(\theta_r)$ has one peak at $\theta_r = \pi/2$. The $P(\theta_r)$ distributions show that $k-j'$ correlation is very weak. The $P(\phi_r)$

The $P(\theta_r)$ distribution describes the $k-j'$ correlation, which is plotted in Figure 4. It is very clearly that for 0.6 eV or 1.0 eV, $P(\theta_r)$ has no sharp peak at $\theta_r = \pi/2$, while for 1.4 eV, $P(\theta_r)$ has one peak at $\theta_r = \pi/2$. The $P(\theta_r)$ distributions show that $k-j'$ correlation is very weak. The $P(\phi_r)$

The $P(\theta_r)$ distribution describes the $k-j'$ correlation, which is plotted in Figure 4. It is very clearly that for 0.6 eV or 1.0 eV, $P(\theta_r)$ has no sharp peak at $\theta_r = \pi/2$, while for 1.4 eV, $P(\theta_r)$ has one peak at $\theta_r = \pi/2$. The $P(\theta_r)$ distributions show that $k-j'$ correlation is very weak. The $P(\phi_r)$

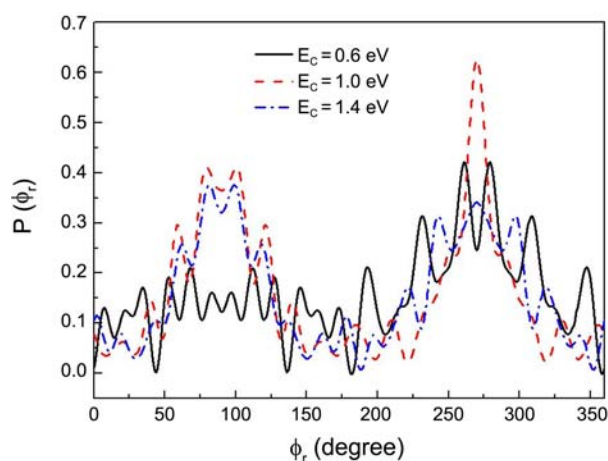


Figure 5. The dihedral angle distribution of $P(\phi_r)$ with respect to the k, k' plane.

distributions are shown in Figure 5. It describes $k-k'-j'$ correlations. There are two peaks in $\pi/2$ and $3\pi/2$. The $P(\phi_r)$

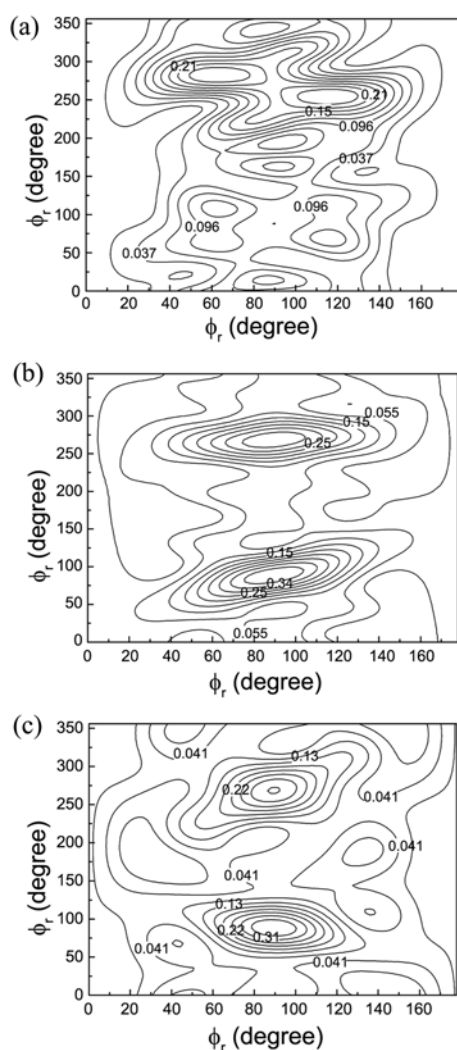


Figure 6. Polar plots of $P(\theta_r, \phi_r)$ distribution at three different collision energies (a) $E_c = 0.6$ eV, (b) $E_c = 1.0$ eV, (c) $E_c = 1.4$ eV over averaged over all scattering angles.

tend to be very asymmetric with respect to the $k-k'$ scattering plane (or about $\phi_r = \pi$), directly reflecting the polarization of angular momentum for three different collision energies. As apparent from the figure, there is no obvious single peak of $P(\phi_r)$ for the three different collision energies, but the average value of $P(\phi_r)$ appearing at the angle close to $3\pi/2$ is evidently larger for 0.6 eV and 1.0 eV, which indicates the trend of the product rotational angular momentum vector j' being oriented along the negative y -axis for both collision energies. However, for 1.4 eV, the average value of $P(\phi_r)$ appearing at the angle close to $\pi/2$ is slightly larger than $3\pi/2$, so that j' is oriented along the positive y -axis, but the degree of orientation is small. The broad distribution of $P(\phi_r)$ indicates that the reaction is mainly dominated by out-of-plane mechanism, in which the product molecule prefers rotating in a plane perpendicular to the scattering plane.

In Figure 6, we also plot the angular momentum polarization in the form of polar plots in θ_r and ϕ_r averaged over all scattering angles. The distributions of $O(\theta_r, \phi_r)$ are in good accordance with the distributions of $P(\phi_r)$ and $P(\phi_r)$ of the NeH^+ products for three collision energies. This reaction belongs to Heavy-Light-Light (HLL) mass combination, which leads to the fact that the product orbital angular momentum is large, and the reactant orbital angular momentum has less influence on the product rotational alignment, which is also consistent with the previous prediction.¹⁷

The $P(\theta_r)$ and $P(\phi_r)$ distributions of NeH^+ product from the reaction $\text{Ne} + \text{H}_2^+ (\nu = 1, 2, 4, j = 0) \rightarrow \text{NeH}^+ + \text{H}$ at a collision energy of 1.0 eV are shown in Figure 7 and Figure 8 respectively. The excitation of the initial HH^+ vibration has a big impact on the stereo-dynamics. From the plot, we can see that the $P(\theta_r)$ and $P(\phi_r)$ distributions of NeH^+ change dramatically when the HH^+ vibration is excited to the $\nu = 1, 2, 3$ energy levels. In Figure 7, the influence of the vibration quantum number on the $P(\theta_r)$ distribution is shown. It is clear that the peak value of $P(\theta_r)$ becomes larger and the distribution becomes narrower when the vibrational quantum number is changed from 1 to 4, which indicates the

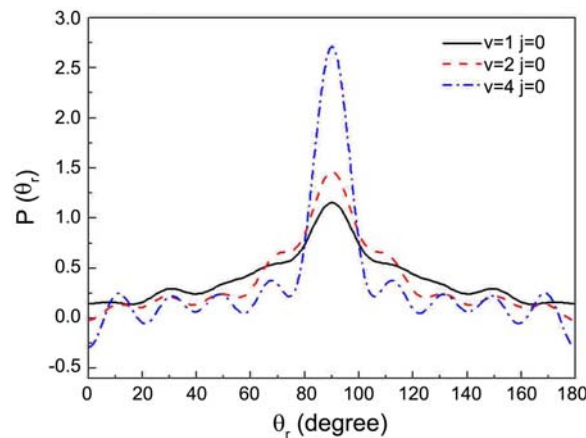


Figure 7. The distribution of $P(\theta_r)$ for NeH^+ product from the reaction $\text{Ne} + \text{H}_2^+ (\nu = 1, 2, 4, j = 0) \rightarrow \text{NeH}^+ + \text{H}$ at the collision energy of 1.0 eV.

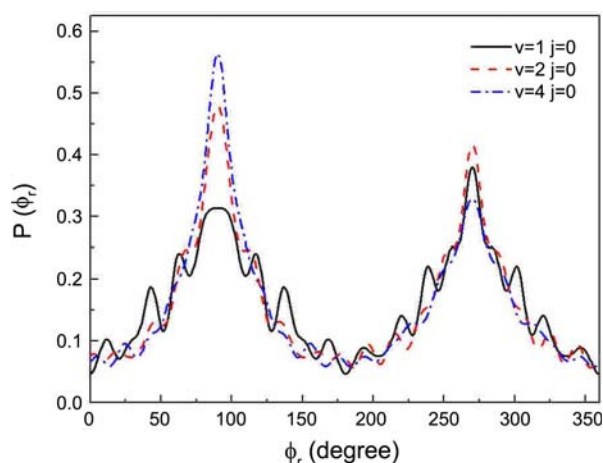


Figure 8. The distribution of $P(\phi_r)$ for NeH^+ product from the reaction $\text{Ne} + \text{H}_2^+$ ($\nu = 1, 2, 4, j = 0$) $\rightarrow \text{NeH}^+ + \text{H}$ at the collision energy of 1.0 eV.

regent vibrational excitation makes the product polarized along the direction at right angle to \mathbf{k} stronger. As shown in Figure 8, for $\nu = 1$, the product slightly orient to the negative y -axis, while for $\nu = 2, 4$, the product obviously orient to the positive y -axis, and the higher vibration level is, the stronger orientation is.

Conclusion

The QCT calculation for the dynamics of the reaction $\text{Ne} + \text{H}_2^+ \rightarrow \text{NeH}^+ + \text{H}$ based on the $1^2 A'$ PES has been performed. The result of reaction probability as a function of collision energy of $\text{Ne} + \text{H}_2^+$ ($\nu = 0, j = 0$) $\rightarrow \text{NeH}^+ + \text{H}$ reaction has been found to be consistent with the TDWP result calculated by Lv *et al.*¹⁹ In addition, the stereodynamics of the title reaction have also been studied. The calculated PDDCSs indicate that the products are mainly forward scattering, and with the increasing collision energy, the tendency of forward scattering decreases to some extent. As the result of the well in the $1^2 A'$ PES, the collision energy hardly affect the polarization of the product rotational angular momentum vector \mathbf{j}' , while the vibrational excitation of reactant has a bigger impact on both alignment and orientation of \mathbf{j}' .

Acknowledgments. This study was supported by the State Key Laboratory of Molecular Reaction Dynamics, Dalian Institute of Chemical Physics, Chinese Academy of Sciences.

Many thanks to Shuangjiang. Lv for providing the potential energy surface, and Prof. Keli Han for providing the code.

References

1. Bilotta, R. M.; Farrar, J. M. *J. Chem. Phys.* **1981**, *75*, 1776.
2. Van Pijkeren, D.; Boltjes, E.; Eck, J. V.; Niehaus, A. *Chem. Phys.* **1984**, *91*, 293.
3. Herman, Z.; Koyano, I. *J. Chem. Soc., Faraday Trans. 2* **1987**, *83*, 127.
4. Zhang, T.; Qian, X.-M.; Tang, X. N.; Ng, C. Y.; Chiu, Y.; Levandier, D. J.; Miller, J. S.; Dressler, R. A. *J. Chem. Phys.* **2003**, *119*, 10175.
5. Dressler, R. A.; Chiu, Y.; Levandier, D. J.; Tang, X. N.; Hou, Y.; Chang, C.; Houchins, C.; Xu, H.; Ng, C. Y. *J. Chem. Phys.* **2006**, *125*, 132306.
6. González-Sánchez, L.; Gómez-Carrasco, S.; Aguado, A. *J. Chem. Phys.* **2004**, *121*, 309.
7. Gómez-Carrasco, S.; Roncero, O.; González-Sánchez, L. *J. Chem. Phys.* **2005**, *123*, 114310.
8. Kuntz, P. J.; Roach, A. C. *J. Chem. Soc., Faraday Trans. 2* **1972**, *68*, 259.
9. González, M.; Blasco, R. M.; Giménez, X.; Aguilar, A. *Chem. Phys.* **1996**, *209*, 355.
10. Huarte-Larrañaga, F.; Giménez, X.; Lucas, J. M.; Aguilar, A.; Launay, J.-M. *J. Phys. Chem. A* **2000**, *104*, 10227.
11. Pendergast, P.; Heck, J. M.; Hayes, E. F.; Jaquet, R. *J. Chem. Phys.* **1993**, *98*, 4543.
12. Urban, J.; Jaquet, R.; Staemmler, V. *Int. J. Quantum Chem.* **1990**, *38*, 339.
13. Kress, J. D.; Walker, R. B.; Hayes, E. F.; Pendergast, P. *J. Chem. Phys.* **1994**, *100*, 2728.
14. Huarte-Larrañaga, F.; Giménez, X.; Lucas, J. M.; Aguilar, A.; Launay, J.-M. *Phys. Chem. Chem. Phys.* **1999**, *1*, 1125.
15. Gilibert, M.; Blasco, R. M.; González, M.; Giménez, X.; Aguilar, A.; Last, I.; Baer, M. *J. Phys. Chem. A* **1997**, *101*, 6821.
16. Gilibert, M.; Giménez, X.; Huarte-Larrañaga, F.; González, M.; Aguilar, A.; Last, I.; Baer, M. *J. Chem. Phys.* **1999**, *110*, 6278.
17. Han, K. L.; He, G. Z.; Lou, N. Q. *J. Chem. Phys.* **1996**, *105*, 8699.
18. Mayneris, J.; Sierra, J. D.; González, M. *J. Chem. Phys.* **2008**, *128*, 194307.
19. Lv, S. J.; Zhang, P. Y.; Han, K. L.; He, G. Z. *J. Chem. Phys.* **2010**, *132*, 014303.
20. Aguado, A.; Paniagua, M. *J. Chem. Phys.* **1992**, *96*, 1265.
21. Chen, M. D.; Han, K. L.; Lou, N. Q. *J. Chem. Phys.* **2003**, *118*, 4463.
22. Wang, M. L.; Han, K. L.; He, G. Z. *J. Chem. Phys.* **1998**, *109*, 5446.
23. Chen, M. D.; Han, K. L.; Lou, N. Q. *Chem. Phys. Lett.* **2002**, *357*, 483.
24. Wrede, E.; Schnieder, L.; Welge, K. H.; Aoiz, F. J.; Bañares, L.; Castillo, J. F.; Martínez-Haya, B.; Herrero, V. J. *J. Chem. Phys.* **1999**, *110*, 9971.
25. Aoiz, F. J.; Brouard, M.; Enriquez, P. A. *J. Chem. Phys.* **1996**, *105*, 4964.